Proceedings of the 50th International School & Conference on the Physics of Semiconductors

The Biological Activity of ZnO Nanostructures Doped by Mg and Co

L. Myroniuk[a,*], D. Myroniuk[a], V. Karpyna[a], O. Bykov[a], I. Garmasheva[b], O. Povnitsa[b], L. Artiukh[b], K. Naumenko[b], S. Zahorodnia[b] and A. Ievtushenko[a]

[a]*I.M. Frantsevich Institute for problems in materials science, NAS of Ukraine, 3 Krhyzhanovsky st., 03142 Kyiv, Ukraine*
[b]*D.K. Zabolotny Institute of Microbiology and Virology, NAS of Ukraine, 154 Zabolotny str., 03143 Kyiv, Ukraine*

Doi: 10.12693/APhysPolA.142.651 *e-mail: liliiamolotovska@gmail.com

Pure, Mg-doped and Co-doped ZnO nanostructures were grown by atmospheric pressure metal-organic chemical vapor deposition. The influence of magnesium and cobalt contained in ZnO on microstructure, cytotoxicity, and virucidal and antibacterial activities under non-irradiated conditions was investigated. The incorporation of Mg and Co impurities into the crystal lattice of ZnO nanostructures modifies their electronic structure, surface morphology, and the concentration of point defects, which have some influence on the biological activity of the prepared ZnO nanostructures. The addition of magnesium and cobalt to ZnO nanostructures did not inhibit the reproduction of type 2 adenovirus, but an increased virucidal action for Mg- and Co-doped ZnO nanostructures against influenza A (H1N1) virus (strain FM/1/47) was observed. The titer of influenza virus was reduced by 1.92 lg for Mg-doped ZnO nanostructures. At the same time, Co-doped ZnO nanostructures showed the best results: the titer reduction was 3.57 for ZnO-Co (10 wt%) and 3.14 lg for ZnO-Co (5 wt%), indicating their good virucidal action. All tested ZnO nanostructures exhibited toxicity towards *E. coli* cells.

topics: ZnO nanostructures, doping, cytotoxicity effect, antimicrobial activity

1. Introduction

Zinc oxide (ZnO), due to its unique physicochemical properties, biocompatibility and availability of synthesis methods, has been considered as a prospective material for a wide range of applications, from the production of semiconductor and optoelectronic devices to biomedical devices [1, 2]. Recently, ZnO has also attracted attention as effective photocatalytic material [3–5]. However, intrinsic ZnO cannot be directly utilized as an effective photocatalytic material because of its poor optical properties that can be improved by doping. The concentration of the main point defects in ZnO, such as oxygen vacancies and zinc interstitials, can be changed by doping. Oxygen vacancies can act as efficient electron traps and lead to an enhancement in the photocatalytic efficiency of the material [1]. The doping itself enhances the versatility of zinc oxide nanostructures for the above-mentioned applications [6].

An environmentally friendly and inexpensive Mg-doped ZnO system is being investigated due to the widening of the band gap of ZnO by alloying with MgO. Similar ionic radii of Zn^{2+} and Mg^{2+} enable the formation of a solid solution despite the lattice mismatch between the structures of ZnO (hexagonal wurtzite) and MgO (cubic periclase) [7]. By changing the Mg-content in $Zn_{1-x}Mg_xO$ from 0 to 1, the direct band gap of the semiconductor could be adjusted from 3.37 to 7.8 eV [8]. Doping with transition metal ions is one of the methods used to increase the efficiency of ZnO absorption in the visible spectrum of radiation by narrowing the band gap. In addition, the photogenerated carriers are captured by localized states of transition metal, which reduces their recombination and ultimately leads to an improvement of the photocatalytic activity of ZnO [9]. Cobalt doping has attracted the attention of researchers in particular because of the proximity of the ionic radii of cobalt and zinc. The effective ionic radius of Co^{2+} is slightly smaller than the radius of Zn^{2+}, so the Co^{2+} ion easily replaces the Zn^{2+} ion in the ZnO lattice without any significant distortion of the ZnO lattice [10].

Knowledge about the kind of doping impurity and its rational concentration is necessary to create an effective photocatalytic material. Besides,

it was reported that the incorporation of Mg ions inside the ZnO matrix enhanced the antibacterial activity against Gram-negative and Gram-positive bacteria such as *Escherihia coli* and *Staphylococcus aureus* [11].

Co-doped ZnO materials with controllable band structure are particularly attractive because of the abundant electronic states of Co and the minor effect of Co on the structure of ZnO [12]. The obtained results in [13] indicate that Co^{2+} ions were substitutionally incorporated into Zn^{2+} sites within the ZnO lattice in ZnO:Co films. Highly photocatalytically active Co-doped ZnO films can be widely used in photocatalysis using visible light to overcome the organic pollution of water and air. Furthermore, the creation of photocatalysts in the form of coatings is promising in terms of their application as antimicrobial surfaces that induce microbial degradation of organic pollution under specific illumination conditions. The application of appropriate antimicrobial surfaces can decrease high number of healthcare-related infections and, the spread of antibiotic-resistant microorganisms [14].

In this paper, we consider the incorporation of Mg and Co metals into ZnO nanostructures (NS) and study the biological activity under non-irradiated conditions (cytotoxicity effect, virucidal and antimicrobial activities) depending on the concentration of doping elements.

2. Experimental

2.1. Synthesis of the ZnO and ZnO-M nanostructures (M = Mg, Co)

The materials used for the synthesis were zinc acetylacetonate ($Zn(C_5H_7O_2)_2$ (with purity > 99.9%, J&K Scientific LTD), magnesium acetylacetonate $Mg(C_5H_7O_2)_2$, and cobalt acetylacetonate $Co(C_5H_7O_2)_2 \cdot 2H_2O$ (with purity > 98%, Tokyo Chemical Industry Co., LTD (TCI)). For deposition of ZnO NS, substrates of a 1×1 cm^2 p-Si (100) (the area of 1 cm^2) were used.

Pure ZnO NS and Mg- and Co-doped ZnO NS were grown on Si substrates by atmospheric pressure metal-organic chemical vapor deposition (APMOCVD) [15]. Powder mixtures of zinc acetylacetonate with magnesium acetylacetonate or cobalt acetylacetonate in the amount of 5 wt% and 10 wt% were used as precursors for grown Mg- and Co-doped ZnO NS, respectively. The deposition process takes place in a tubular furnace with a temperature gradient between two zones: the high-temperature zone of 500–600°C, which is used for placing the Si substrate, and the low temperature zone of 190–250°C for the evaporation of precursors mixture. The Si substrate were previously cleaned with ethanol and deionized water, and then dried with an air flow [16]. Then, the Si substrates were positioned in a horizontal quartz tube (reactor) with a diameter of 26 mm and a length of 350 mm, at a distance of about 180–200 mm from the edge of the furnace. A powder mixture of Mg acetylacetonate/Zn acetylacetonate or Co acetylacetonate/Zn acetylacetonate, having a total mass of 1 g, was put in a ceramic evaporation boat, which was placed in the reactor chamber at a distance of 50 mm from the edge of the furnace. The deposition time was about 60 min. After that, the Si substrates coated by ZnO NS (pure or Mg-, Co-doped), were unloaded from the furnace for characterization.

For simplicity, the prepared magnesium-doped ZnO samples with the concentrations 5 wt% and 10 wt% were called ZnO-Mg (5 wt%) and ZnO-Mg (10 wt%), respectively. Similarly for cobalt-doped ZnO, the samples were named ZnO-Co (5 wt%) and ZnO-Co (10 wt%).

2.2. Characterization

The crystal structure of the prepared ZnO samples were characterized using a DRON-3M X-ray diffractometer in Bragg-Brentano configuration using Cu K_α radiation of a wavelength of 1.54056 Å in the θ–2θ range from 30 to 90°. A scanning electron microscope (SEM) named Tescan Mira 3 LMU SEM, with a primary beam acceleration potential of 20 kV, was chosen to investigate the morphology of the obtained NS. Additionally, the installed energy dispersion X-ray (EDX) spectrometer made it possible to determine the local elemental composition of the grown nanostructures.

2.3. Microbiology experiment

2.3.1. Viruses, cell and bacteria cultures

Cell cultures MDCK (Madin-Darby Canine Kidney cells) and Hep-2 (Larynx Epidermoid Carcinoma) were used in experiments [17]. Influenza A virus (H1N1) (strain FM/1/47) and human adenovirus serotype 2 (HAdV2) were obtained from the collection of the Institute of Epidemiology and Infectious Diseases of the Academy of Medical Sciences of Ukraine and the Institute of Microbiology, Medical University of Budapest, respectively. Antibacterial activity was investigated by using Gram-negative bacteria *Escherichia coli* strain UCM-906 (ATCC 25922).

2.3.2. Cytotoxicity, virucidal and antibacterial activity study

To study the cytotoxic effect of the nanostructures, first, their washes were obtained by placing the structures in the wells of a 24-well plate with 1 ml of DMEM medium (Biowest, France). The plate was placed at 37°C in an atmosphere of 5% CO_2 for 24 h. The washes were selected and a series of ten-fold dilutions were prepared. Cell cultures in a 96-well plate were washed from the culture medium after 1 day of growth and formation of 70–90% of the monolayer. The diluted washes were added at 100 μl/well in triplicate. Wells with DMEM medium were used as a cell control. The

plates were kept for 72 h at 37°C in an atmosphere of 5% CO_2. Cell viability was studied using MTT solution (Sigma, USA) according to standard methods [18].

To study the virucidal effect, the undoped and doped ZnO nanostructure were placed in the wells of a 24-well plate, and 50 μl of undiluted virus-containing material was applied to the surface of the nanomaterial. A square of Parafilm M (Bemis, USA) with an area of 1 cm^2 was covered on top to prevent drying of the material and better contact of the virus with the nanostructure surface. The plate was kept for 1 h in the dark at room temperature and 450 μl/well of support medium was added. The virus was suspended and selected for study, preparing a series of 10-fold dilutions. Further study of the virucidal effect of nanostructures was carried out according to the classical method. Cells were cultured for 72 h until a pronounced cytopathogenic effect (CPE) was formed in control of the virus. A decrease in the infectious titer of the virus by 1.5–2 lg $TCID_{50}$/ml and more, compared with the control of the virus, indicates a virucidal effect [19].

The antibacterial activity of Mg (Co)-doped ZnO NS were investigated using Gram-negative bacteria *E.coli*. Bacteria were grown in casein soy broth for 24 h at 37°C. After incubation, the bacterial culture was centrifuged and the bacterial suspension at a concentration of 10^5 CFU/ml was prepared from the pellet with sterile distilled water. One milliliter of the suspension was added to the wells of a 24 well plate. The investigated samples were immersed in the bacterial suspension and kept at room temperature (24°C) under dark conditions. The viability of *E. coli* cells was determined after 2, 3, 4, 5, and 24 h using the 10-fold dilution method. The dilutions were spread onto casein soy agar plates which were incubated at 37°C for 24 h, and colonies forming units (CFU) were then counted. The initial bacterial suspension without nanostructure sample was used as a control. All experiments were performed in duplicates. Data processing was performed using Statistika 7.0 software by employing the analysis of variance (ANOVA) followed by LSD test ($P < 0.05$). Data on bacterial growth inhibition are presented as mean ± standard error.

3. Results and discussion

Figure 1 shows XRD patterns of undoped ZnO NS and Mg-doped (Co-doped) ZnO NS. XRD patterns confirm the formation of ZnO NS with a wurtzite type of crystalline phase. Intense XRD reflections are seen from planes (100), (002), (101), and (110).

The absence of additional phases, as well as the lack of shifting of the reflexes maxima into higher θ–2θ angles, indicates the incorporation of magnesium ions into cation sublattice of ZnO with the substitution of zinc ions. This slight change in ZnO lattice modifies its electronic band structure and introduces crystal defects [20]. XRD patterns for Co-doped ZnO NS also confirm the formation of the crystalline phase of wurtzite ZnO with the most intense reflections from planes (100), (002), (101) and (110). The absence of the secondary phase like CoO, Co, and Co_3O_4 indicates that Co mainly incorporates into the ZnO cation sublattice.

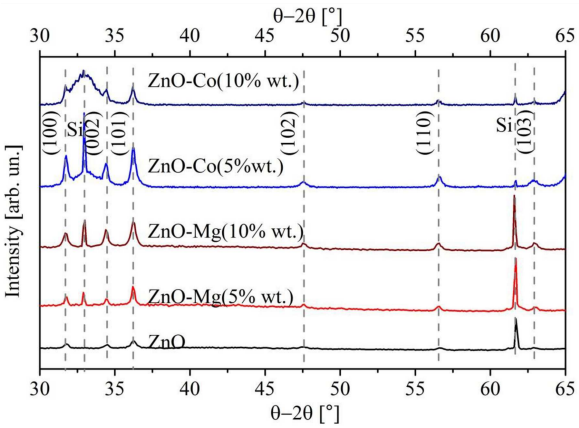

Fig. 1. XRD pattern for pure ZnO NS and Mg-doped (Co-doped) ZnO NS.

TABLE I

Elemental analysis of Mg- and Co-doped ZnO NS.

Sample	Atomic consist [%]					
	C	O	Si	Zn	Mg	Co
ZnO	25.23	38.43	2.78	33.57	–	–
ZnO-Mg (5 wt%)	27.34	31.57	18.77	21.28	–	–
ZnO-Mg (10 wt%)	24.73	35.84	11.97	23.56	3.90	–
ZnO-Co (5 wt%)	15.88	37.76	3.48	38.12	–	4.76
ZnO-Co (10 wt%)	13.52	38.64	2.40	36.88	–	8.57

SEM images of the Mg- and Co-doped ZnO NS are shown in Fig. 2. The SEM micrographs of ZnO-Mg films show that the surface is relatively porous. The presented SEM images indicate that Mg doping inhibits the growth of ZnO, which leads to the formation of smaller nanostructures with a larger surface area.

From the presented SEM images of the ZnO-Co films, one can see that the surface of the samples obtained is also relatively porous. The SEM images demonstrate that the increasing doping concentration inhibits the growth of nanostructures, which leads to the formation of structures with smaller size and larger surface area. The size of the ZnO NS was about 100 nm, while at the same time the size of the Co-doped ZnO NS was less than 50 nm.

EDX analysis for deposited Mg- and Co-doped ZnO NS, grown on Si substrates, confirms the presents of doping elements, i.e., magnesium and cobalt (see Table I).

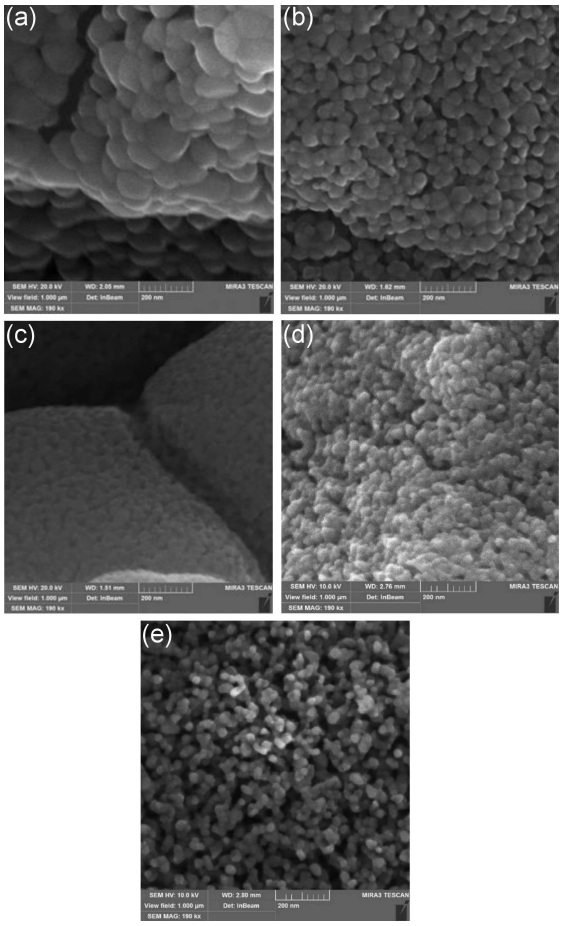

Fig. 2. SEM micrographs for pure ZnO NS and Mg-doped (Co-doped) ZnO NS: (a) ZnO, (b) ZnO-Mg (5 wt%), (c) ZnO-Mg (10 wt%), (d) ZnO-Co (5 wt%), (e) ZnO-Co (10 wt%).

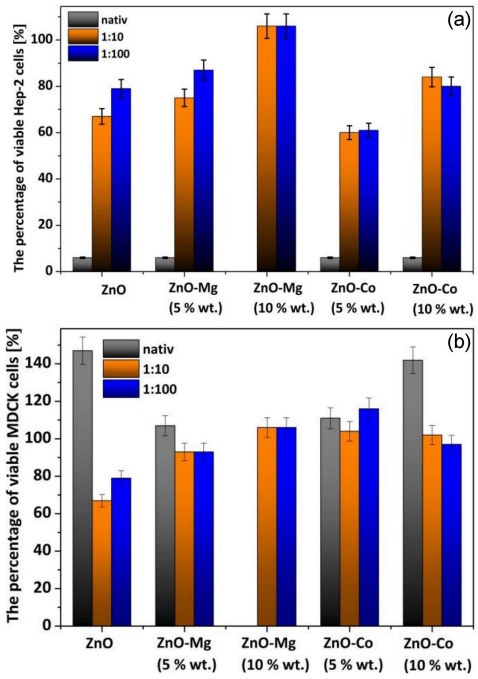

Fig. 3. Cytotoxicity of pure ZnO, ZnO-Mg, and ZnO-Co NS. Toxic effect evaluated by MTT assay after 72 h exposure on (a) Hep-2 and (b) MDCK cells. Values represent the mean ± S.D. for three independent experiments. Control untreated cells — 100% viability.

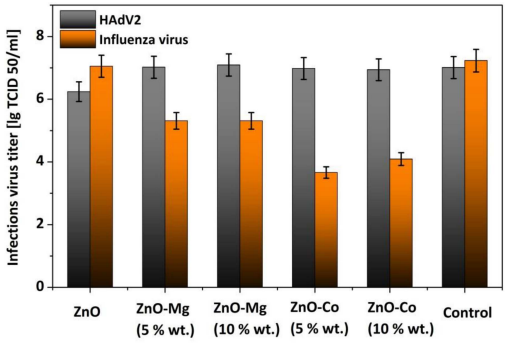

Fig. 4. Infectious titers of human adenovirus type 2 and influenza A virus in the presence of nanocomposites. Virucidal effect of pure ZnO, ZnO-Mg and ZnO-Co NS were evaluated by MTT method after 72 hours of incubation. Values represent the mean value for three independent experiments.

As can be seen in the diagrams (Fig. 3a), the native (undiluted) washes from the nanostructures were toxic to Hep-2 cells; the number of living cells did not exceed 6%. The most toxic was the wash with ZnO-Mg (10 wt%) — no living cells were detected. At 10-fold and 100-fold dilutions, the washes were mildly toxic to Hep-2 cells. The wash with ZnO-Co (5 wt%) was more toxic, with only 60% live cells in 1:10 and 1:100 dilutions.

MDCK cells were more resistant to leaching of zinc oxide nanostructures doped with magnesium and cobalt (Fig. 3b). In the native state, the washes were not toxic to cells, except for ZnO-Mg (10 wt%) NS, which was toxic to both Hep-2 cells and MDCK. Undiluted washes of ZnO and ZnO-Co NS had a stimulating effect on the proliferation of MDCK cells.

A study of the virucidal activity of ZnO NS against human adenovirus serotype 2 showed that the ZnO samples were active by reducing the virus titer by 0.75 lg (Fig. 4). The addition of magnesium and cobalt to ZnO did not inhibit virus reproduction; on the contrary, the virus titers increased and were close to the virus control.

A completely different picture was observed when influenza A (H1N1) virus (strain FM/1/47) was used as the viral model. Due to the lack of the influence of ZnO NS on the infectious titer of the influenza virus (Fig. 4), the addition of magnesium and cobalt led to an increase in the virucidal effect of nanostructures. Mg-doped ZnO NS reduced the influenza virus titer by 1.92 lg, and Co-doped ZnO NS by 3.14 lg (for ZnO-Co (10 wt%)) and 3.57 (for ZnO-Co (5 wt%)), which indicates their strong

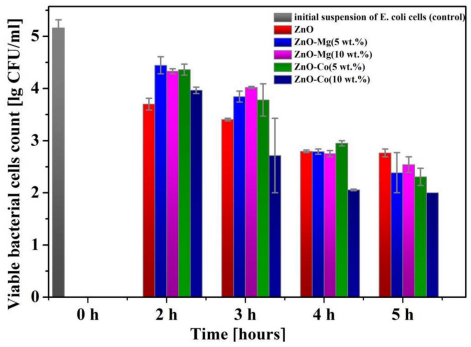

Fig. 5. Effect of ZnO NS and Mg-doped (Co-doped) ZnO NS on the viability of *E. coli* cells.

virucidal effect. As can be seen from the above results, the amount of metal practically did not change the virucidal effect in NS, nevertheless, the presence of the metal was important. Here, cobalt-doped NS had greater virucidal activity. The virucidal effect of nanostructures increased with a decrease in their size (from 100 to 50 nm).

The antibacterial activity of Mg- and Co-doped ZnO NS against *E. coli* under dark conditions was investigated. The aqueous bacterial suspension was used to prevent the decrease of ZnO toxicity due to the interaction of ZnO NS with organic components of the culture medium, as shown by the authors [21]. It was observed that all NS tested exhibited toxicity towards *E. coli* cells. The number of viable cells evaluated by colony counting method was about 1000-fold reduced as compared to the initial concentration of bacterial cells (10^5 CFU/ml) upon incubation with nanostructures after 5 h. After 24 h incubation with the nanostructures, there were no surviving *E. coli* cells in the aqueous suspensions, while only a slight decrease was observed in the control suspension. Figure 5 shows the effect of ZnO NS and Mg-doped (Co-doped) ZnO NS on the viability of bacterial cells after 5 h of incubation. It should be noted that after 2–3 h of incubation, ZnO NS exhibited higher antibacterial activity than metal-doped ZnO NS. The viable bacterial cell count was 65% of the initial value, while for Mg- and Co-doped ZnO NS it was 72–76% and 65–74%, respectively. The weaker antibacterial effect of the doped ZnO NS may be mediated by a decrease in the ZnO NS toxicity as reported in the literature. For example, the authors showed that the toxicity of ZnO nanoparticles decreased when ZnO was doped with biocompatible Mg^{2+} ions [22]. After 5 h incubation, Mg-doped ZnO NS did not exhibit high antibacterial activity compared to ZnO NS. At the same time, doping of ZnO NS with Co at a concentration of 1–10 wt% increases the antibacterial activity.

Thus, the obtained results correspond to the data of other authors on the antibacterial properties of pure ZnO and Mg- and Co-doped ZnO NS [21, 23, 24]. A further detailed study is needed to elucidate different antibacterial kinetic of doped ZnO with respect to pure ZnO NS during 3 h of incubation and the mechanism of antibacterial action under dark conditions.

4. Conclusions

The effect of magnesium and cobalt doping in the target structures ZnO-Mg and ZnO-Co, respectively, grown by the APMOCVD method on Si substrates has been studied. It has been shown that the incorporation of Mg and Co into the ZnO structure modifies its properties by increasing the surface area and the occurrence of crystal defects.

Studies of virucidal activity of metal-doped ZnO NS showed a decrease in the titer of influenza A virus by 1.92 lg for ZnO-Mg NS, and for Co-doped ZnO NS, the titer decrease was 3.14–3.57 lg. Therefore, as the size of nanoparticles decreased, their virucidal effect increased. The difference in virucidal effect of the structures is most likely related to the ability to destroy the lipid envelope of the influenza virus, in contrast to adenovirus that does not contain it. Therefore, metal-doped ZnO nanostructures have prospects for use against viruses with a lipid envelope, including SARS-Cov-2.

Mg- and Co-doped zinc oxide NPs were toxic to Hep-2 cells in the undiluted state and non-toxic in dilutions, indicating a dose-dependent cytotoxic effect. All nanostructures, except ZnO-Mg (10 wt%), were not toxic to MDCK cells. Undiluted washes of ZnO NS and ZnO-Co NS had a stimulating effect on the proliferation of MDCK cells.

All metal-doped ZnO NS showed antibacterial activity against *Escherichia coli* when investigated under non-irradiated conditions.

Therefore, all the results obtained are perspectives for the development of effective antimicrobial ZnO-based coatings. Additional investigations are needed to "install" the influence of ZnO-doped nanostructures photocatalytic effect against bacteria and viruses.

Acknowledgments

We express many thanks to all Polish people and the Organizers of "Jaszowiec 2022" conference for Solidarity with Ukraine in this hard time. Also, we are very grateful to the Armed Forces of Ukraine for giving us the opportunity to prepare this article. This work was partially supported by the research projects of the NAS of Ukraine "The development of photocatalytic nanocomposites for viruses inactivation in the air".

References

[1] O.E. Baibara, M.V. Radchenko, V.A. Karpyna, A.I. Ievtushenko, *Phys. Chem. Solid State* **22**, 585 (2021).

[2] A.A. Essawy, I.H. Alsohaimi, M.S. Alhumaimess, H.M.A. Hassan, M.M. Kamel, *J. Environ. Manage.* **271**, 110961 (2020).

[3] M. Samadi, M. Zirak, A. Naseri, E. Khorashadizade A.Z. Moshfegh, *Thin Solid Films* **605**, 2 (2016).

[4] C.B. Ong, L. Yong, A.W. Mohammad, *Renew. Sust. Energ. Rev.* **81**, 536 (2018).

[5] K. Qi, B. Cheng, J. Yu, W. Ho, *J. Alloys Compd.* **727**, 792 (2017).

[6] S. Kumaresan, K. Vallalperuman, S. Sathishkumar, M. Karthik, P. SivaKarthik, *J. Mater. Sci. Mater. Electron.* **28**, 9199 (2017).

[7] T.B. Ivetić, M.R. Dimitrievska, N.L. Finčur, L.R. Đačanin I.O. Gúth B.F. Abramović S.R. Lukić-Petrović, *Ceram. Int.* **40**, 1545 (2014).

[8] V. Etacheri, R. Roshan, V. Kumar, *ACS Appl. Mater. Int.* **4**, 2717 (2012).

[9] M. Adeel, Ŕ. Saeed, I. Khan, M. Muneer, N. Akram, *ACS Omega* **6**, 1426 (2021).

[10] W. Vallejo, A. Cantillo, B. Salazar, C. Diaz-Uribe, W. Ramos, E. Romero, M. Hurtado, *Catalysts* **10**, 528 (2020).

[11] S. Mahmud, A. Seeni, N.H.M Kaus, L.C. Ann, S.K.M. Bakhori, H. Hasan, D. Mohamad, *Nano-Micro Lett.* **7**, 219 (2015).

[12] D.Y. Inamdar, A.D. Lad, A.K. Pathak, I. Dubenko, N. Ali, S. Mahamuni, *J. Phys. Chem. C* **114**, 1451 (2010).

[13] O.A. Yildirim, H. Arslan, S. Sonmezogly, *Appl. Surf. Sci.* **390**, 111 (2016).

[14] M. Visnapuu, M. Rosenberg, E. Truska et al., *Colloids Surf. B Biointerfaces* **169**, 222 (2018).

[15] D.V. Myroniuk, L.A. Myroniuk, V.A. Karpyna, L.I. Petrosian, A.I. Ievtushenko, *J. Nano- Electr. Phys.* **13**, 05008 (2021).

[16] S. Golovynskyi, A. Ievtushenko, S. Mamykin et al., *Vacuum* **153**, 204 (2018).

[17] *European Collection of Animal Cell Cultures Catalog*, PHLS Centre of Applied Microbiology and Research, Salisbury (UK) 1990.

[18] Y.T. He, J. Wan, T. Tokunaga, *J. Nanopart. Res.* **10**, 321 (2008).

[19] L.K Kohn, M.A. Foglio, R.A. Rodrigues, I.M. Sousa, M.C. Martini, M.A. Padilla, *Braz. J. Poultry Sci.* **17**, 275 (2015).

[20] M. Samadi, M. Zirak, A. Naseri, E. Khorashadizade, A.Z. Moshfeghet, *Thin Solid Films* **605**, 2 (2016).

[21] L. Mei, Z. Lizhong, L. Daohui, *Environ. Sci. Technol.* **45**, 1977, (2011).

[22] S. Auger, C. Henry, C. Péchoux, S. Suman, N. Lejal, N. Bertho, T. Larcher, S. Stankic, J. Vidic, *Sci. Rep.* **8**, 12276 (2018).

[23] G. Poongodi, P. Anandan, M. R. Kumar, R. Jayavel, *Spectrochim. Acta Part A Mol. Biomol. Spectr.* **148**, 237 (2015).

[24] G. Kasi, J. Seo, *Mater. Sci. Eng. C* **98**, 717 (2019).